JOURNAL OF Materials CHEMISTRY

New lead triphosphonates: synthesis, properties and crystal structures

Aurelio Cabeza, Miguel A. G. Aranda and Sebastian Bruque*

Departamento de Química Inorgánica, Cristalografía y Mineralogía, Universidad de Málaga, 29071 Málaga, Spain

Received 20th July 1998, Accepted 5th November 1998

Two new lead nitrilotris(methylene)triphosphonates, $Pb[(H_2O_3PCH_2)N(CH_2PO_3H)_2]$ **I** and $Pb_2[(O_3PCH_2)N(CH_2PO_3H)_2]\cdot H_2O$ **II**, have been synthesised. **I** is triclinic, space group $P\bar{1}$, $a=8.5077(2)$, $b=11.2363(3)$, $c=5.9484(2)$ Å, $\alpha=98.802(2)$, $\beta=104.955(1)$, $\gamma=80.911(2)^\circ$, $Z=2$. **II** is monoclinic, space group *Pn*, $a=7.3614(2)$, $b=11.3889(2)$, $c=7.2541(2)$ Å, $\beta=100.389(2)^\circ$ and $Z=2$. Their structures have been solved from laboratory X-ray data by using *ab initio* powder diffraction methodology. The reliability factors were $R_{wP}=9.28\%$, $R_P=7.20\%$ and $R_F=2.67\%$, for **I**, and $R_{wP}=12.51\%$, $R_P=9.38\%$ and $R_F=4.45\%$, for **II**. **I** shows a new layered structure which has small cavities, inside an inorganic layer, in which the hydrogen phosphonate and the dihydrogen phosphonate groups are located. **II** is also layered with the water molecule situated in the interlamellar space. Thermal data, IR data and ion-exchange properties are also reported and discussed. **II** dehydrates to yield orthorhombic $Pb_2[(O_3PCH_2)N(CH_2PO_3H)_2]$ **III**. Hydrolysis of **I** leads to **II**.

Introduction

Metal phosphonate chemistry has attracted substantial research interest in the last fifteen years.[1] Although, the main research effort in the metal phosphonates field was initially directed toward tetravalent cation phosphonates (for instance Zr, Ti, Sn, Ce),[2,3] many other works have been reported concerning the synthesis, crystal structures and properties of divalent,[4–6] and trivalent metal phosphonates.[7–9]

One of the reasons for the rapid growth of research in metal organo-phosphonates is the wide variety of accessible structure types that these materials can show: one-dimensional chains,[10] layered structures[4,5,9] and three-dimensional microporous frameworks.[11] However, their more attractive feature is they allow us to have a certain control over the dimensionality of the metal phosphonates by a suitable choice of the phosphonic acid used as precursor in the synthesis.[12] So, pillared layered phosphonates (PLSs) can be synthesised by using, for example, diphosphonic acids $H_2O_3P–R–PO_3H_2$ as pillaring agents,[13] or by the choice of the functional end Z of the phosphonic acid, $H_2O_3P–R–Z$ ($Z=CO_2H$, NH_2).[14] The use of these functionalized phosphonic acids allows for study not only of how the functionalized end may dictate the dimensionality of the solid, but also the reactivity that these organic functions may show. Consequently, these materials can find a great number of practical applications as catalysts, hosts in intercalation compounds, sorbents, ion exchangers, protonic conductors, and components in the preparation of films possessing optical, non-linear optical or electronic properties.[15]

In this paper, we describe the synthesis, characterisation and crystal structure of two new lead phosphonates, using as precursor nitrilotris(methylene)triphosphonic acid (TPA). The solids obtained were: $Pb[(H_2O_3PCH_2)N(CH_2PO_3H)_2]$ **I** and $Pb_2[(O_3PCH_2)N(CH_2PO_3H)_2]\cdot H_2O$ **II**. We also study the possibility of exchanging the protons from the different hydroxyl groups in **I** and **II** by cations. **II** dehydrates to give $Pb_2[(O_3PCH_2)N(CH_2PO_3H)_2]$ **III**.

Experimental

Chemicals of reagent quality were obtained from Aldrich Chemical Co. and used without purification. Nitrilotris(methylene)triphosphonic acid (TPA) was used as commercial 50 wt.% solution in water. Carbon, nitrogen and hydrogen contents were determined by elemental chemical analysis on a Perkin-Elmer 240 analyser. TG and DTA data were collected on a Rigaku Thermoflex apparatus at the heating rate 10 K min^{-1} in air with calcined Al_2O_3 as internal reference standard in air. IR spectra were recorded on Perkin Elmer 883 spectrometer in the spectral range 4000–400 cm^{-1}, by using dry KBr pellets containing 2 wt.% sample. Room temperature X-ray powder diffraction patterns were collected on a Siemens D-5000, automated diffractometer using graphite-monochromated Cu-Kα radiation. Both samples were diluted and blended with spherical particles of Cab-O-Sil M-5 (Fluka), to avoid/reduce the preferred orientation.[16,17] The angular range scanned was $2\theta=6–90^\circ$, with a step size of 0.02° and a counting time of 15 s per step. The powder thermodiffractometric study was carried out in air with the same diffractometer but in a second goniometer permanently equipped with an HTK10 heating chamber. The samples were packed over the Pt foil that is both the heating system and the holder. The thermodiffractometric patterns were scanned over the angular range $2\theta=4–36^\circ$, with a step size of 0.04° and a counting time of 2 s per step. The appropriate heating and cooling temperatures were selected by using the Diffract AT software. Samples were held at each temperature for 10 min, before recording any pattern, to ensure that any transformations that may take place, were allowed time to do so.

Synthesis of $Pb[(H_2O_3PCH_2)N(CH_2PO_3H)_2]$ I

To 20 ml of TPA solution (50% w/w, 43 mmol) was added another solution containing 5.40 mmol of lead acetate trihydrate dissolved in 50 ml of distilled water. The resulting Pb : TPA molar ratio was 1 : 8. A white precipitate was immediately formed. The suspension was refluxed for 7 days. A powdered single phase was filtered off, washed with water and with acetone, and dried under vacuum. Analytical data for **I**: C, 7.07%; N, 2.86; H, 1.99%; C/N ratio 2.88. Calc.: C, 7.14; N, 2.78; H, 1.98%. C/N ratio 3.00.

Synthesis of $Pb_2[(O_3PCH_2)N(CH_2PO_3H)_2]\cdot H_2O$ II

5 ml of TPA (10.8 mmol) was added, slowly and with constant stirring to 50 ml of a solution containing 16.2 mmol of lead acetate trihydrate. The resulting solution had a Pb : TPA molar ratio 1.5 : 1. Under these conditions, a viscous sol was formed, to which was added another 50 ml of distilled water. The suspension was refluxed for 6 days. A powdered single phase

was filtered off, washed with water and acetone, and finally dried under vacuum. Analytical data for **II**: C, 4.97; N, 1.88; H, 1.23%; C/N ratio 3.08. Calc.: C, 4.94; N, 1.92; H, 1.37%; C/N ratio 3.00. When **II** is heated above 200 °C it dehydrates to give $Pb_2[(O_3PCH_2)N(CH_2PO_3H)_2]$ **III**. Other Pb/TPA ratios were tested, but no single phases were obtained.

Results and discussion

Thermal study

TG–DTA curves for $Pb[(H_2O_3PCH_2)N(CH_2PO_3H)_2]$ **I** and $Pb_2[(H_2O_3PCH_2)N(CH_2PO_3)_2]\cdot H_2O$ **II** are shown in Fig. 1(a) and (b), respectively. The DTA curve for **I** shows four endothermic and one exothermic effects. The sharp exothermic effect observed at 320 °C is due to the combustion of the organic nitrogenated fraction of the sample with the release of NO_x, CO_2 and H_2O gases. The first endothermic effect is sharp and takes place at 265 °C and it may be due to a phase transition just before the loss of the organic moieties. The remaining endotherms are broad and take place at 522 (shoulder), 600, and 950 °C. The latter may correspond to melting/decomposition and release of P_2O_5. The final decomposition product is an amorphous lead phosphate glass. There is no region of constant weight at high temperatures.

For **II** [Fig. 1(b)], there is an initial endotherm centred at 165 °C due to the loss of hydration water (the observed and calculated weight losses are 2.50 and 2.47%, respectively). There is a second endotherm at 345 °C due to a possible phase transition, which is followed by a strong exothermic effect. This exotherm is caused by the combustion of part of the organic matter and is centred at 410 °C. Then, several minor endotherms take place in the range 450–700 °C, probably due to pyrolysis of the remaining organic matter. The final thermal decomposition product at 1000 °C has a powder diffraction pattern that matches that of $Pb_2P_2O_7$ (PDF database no. 13–0273). The overall observed mass loss, 9.75%, agrees well with the theoretical loss of 9.35%, as deduced from the thermal decomposition reaction [eqn. (1)]. Therefore, the solid obtained at high temperature is probably formed by crystalline $Pb_2P_2O_7$ and an amorphous phase with a high P/Pb ratio.

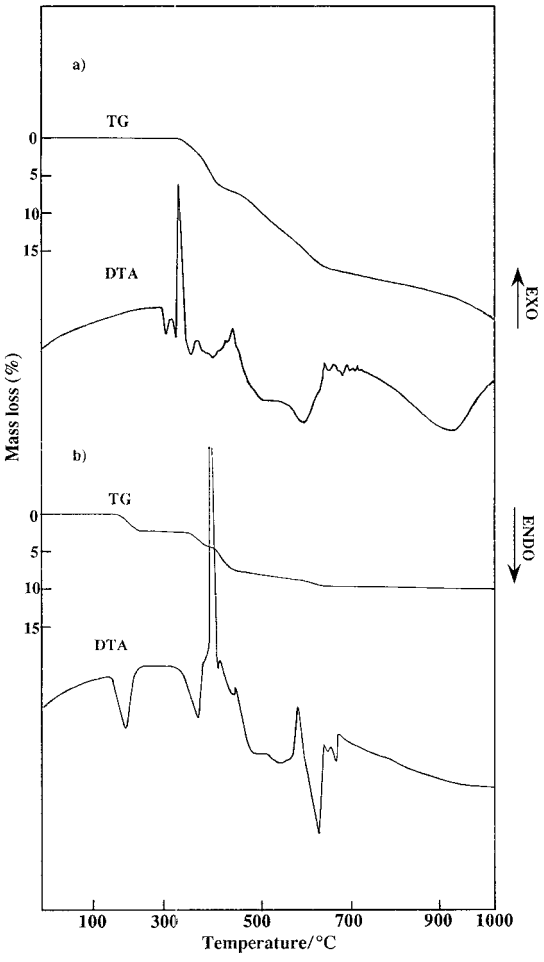

Fig. 1 TG–DTA curves for (a) $Pb[(H_2O_3PCH_2)N(CH_2PO_3H)_2]$ and (b) $Pb_2[(O_3PCH_2)N(CH_2PO_3H)_2]\cdot H_2O$.

$$Pb_2[(O_3PCH_2)N(CH_2PO_3H)_2]\cdot H_2O(s) + 13/2O_2(g) \rightarrow$$
$$Pb_2P_2O_7(s) + 1/2P_2O_5(s) + 3CO_2(g) + NO_2(g) + 5H_2O(g)$$

A thermodiffractometric study of **II** (Fig. 2) was undertaken to characterize the water loss. **II** is only stable up to 150 °C and above this temperature the water starts to be released. Between 160 and 340 °C, $Pb_2[(O_3PCH_2)N(CH_2PO_3H)_2]$ **III** exists as a single phase. Rehydration does not take place even after storing the sample, for several days, in a vessel at 58% relative humidity (obtained from a 40% w/w aqueous solution of H_2SO_4). It is important to point out that the most intense peak of **II**, at 11.39 Å, is slightly displaced to 11.7 Å after the water loss. This increase in the interlayer distance may be caused by a small structural rearrangement after dehydration and this behavior has already been described for other layered metal phosphonates.[18] The similarities in the powder patterns of **II** and **III**, suggest closely related structures.

Ion-exchange study

Because the two lead phosphonates contain two or three acidic hydrogen atoms per formula unit, a study of the possible ion-exchange properties of these compounds by H^+–Li^+ and H^+–Cu^{2+} ion exchange was carried out. 200 mg of each phosphonate (**I** and **II**) were suspended (at 40 °C, under moderate stirring) in 25 ml of $Li(O_2CMe)\cdot 2H_2O$ or $CuCl_2\cdot 2H_2O$ solutions, for three days, with a final molar relation $H^+:Li^+$ or $H^+:Cu^{2+}$ of 1:2. The study was performed in water and in absolute ethanol solutions. No modifications in the X-ray powder diffraction pattern of **II** were observed independently of the metallic salt and the solution used. The results obtained for **I** depend on the pH. If it is suspended in lithium acetate solution in absolute ethanol (pH $\approx$9.7) no (clear) reaction is observed. However, a close inspection of the pattern revealed weak peaks which indicates that **II** was present. Therefore, this indicates a small degree of decomposition of **I** to yield **II**. If the experiment is carried out in aqueous solution and in contact with the lithium salt, pH $\approx$5.3, the powder pattern of the final sample is characteristic of phase **II**. When $CuCl_2\cdot 2H_2O$ is used, pH $\approx$3.7, no modifications in the X-ray diffraction pattern are observed. Also, it is necessary to use an acidic medium to prevent the hydrolysis of **I** and precipitation of copper hydroxide.

IR spectroscopic study

IR spectra were recorded between 4000–400 cm^{-1} and they are shown in Fig. 3(a), (b) and (c) for **I**, **II** and **III**, respectively. The region between 4000 and 1400 cm^{-1} can be selected to study in detail the hydration water and the P–O–H groups. The two bands observed at 2760 and 2340 cm^{-1}, which are likely due to ν(P–OH) and 2δ(P–O–H) respectively, are characteristic of hydrogen phosphonate groups and they are more intense for **I** in accord with its stoichiometry. **II** shows an intense and broad band in the O–H stretching vibration region at 3400 cm^{-1}, which is consistent with the presence of hydration water interacting by H-bonding. The bending H–O–H vibration of the hydration water is located at *ca.* 1620 cm^{-1}, as a sharp band. When **II** is heated above 165 °C to give **III**, the band at 3400 cm^{-1} disappears and a broad band at 1650 cm^{-1} appears. This band may be due to an overtone or combination band of the CPO_3 stretching

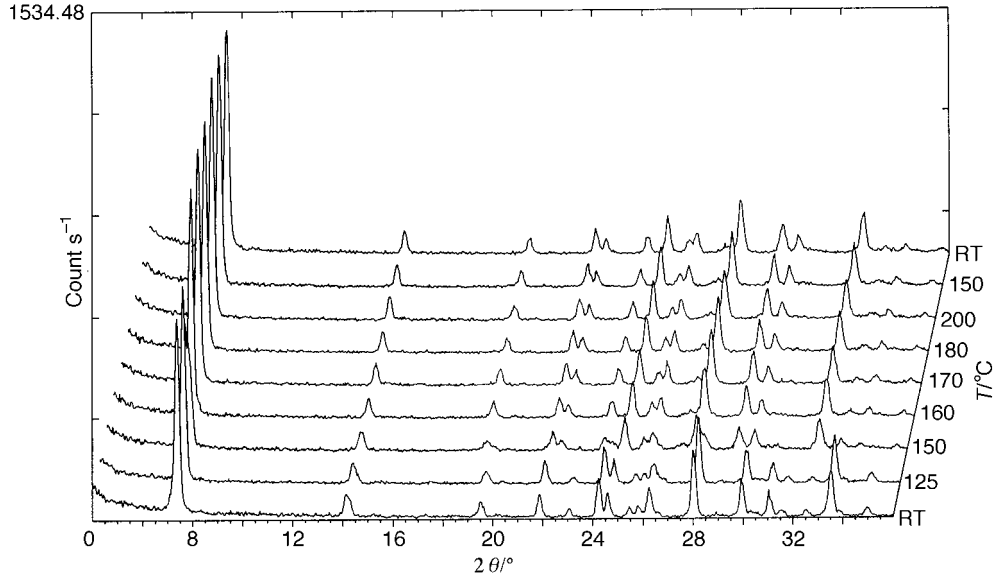

Fig. 2 X-Ray thermodiffractometric pattern for $Pb_2[(O_3PCH_2)N(CH_2PO_3H)_2]\cdot H_2O$.

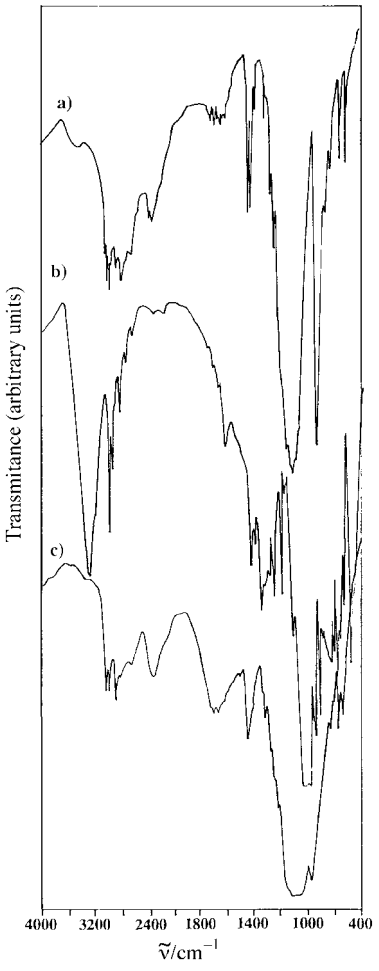

Fig. 3 IR spectra for (a) $Pb[(H_2O_3PCH_2)N(CH_2PO_3H)_2]$, (b) $Pb_2[(O_3PCH_2)N(CH_2PO_3H)_2]\cdot H_2O$ and (c) $Pb_2[(O_3PCH_2)$-$N(CH_2PO_3H)_2]$.

vibrations. Alternatively, the band may be also due to the bending vibration of the PO–H–OP group, which interacts strongly by H-bonding.

Crystal structure study

$Pb[(H_2O_3PCH_2)N(CH_2PO_3H)_2]$. The X-ray laboratory powder pattern was auto-indexed using the TREOR90 program[19] giving a triclinic unit cell with $a=8.494(2)$, $b=11.216(2)$, $c=5.939(1)$ Å, $\alpha=98.79(1)$, $\beta=104.93(2)$, $\gamma=80.95(1)^\circ$, $V=536.2$ Å^3, $Z=2$, V_{at} (non-H atoms)$=15.77$ Å^3 atom^{-1}, $M_{20}=71$[20] and $F_{20}=140$ (0.0046, 31).[21] The crystal structure was solved by *ab initio* powder diffraction procedures. The pattern decomposition option of the GSAS package[22] was used to extract structure factors, using the Le Bail method,[23] from a limited region of the pattern ($6<2\theta<60.8^\circ$). The pattern was fitted without any structural model by refining the overall parameters: background, zero-point error, unit cell and peak shape values. A pseudo-Voigt peak shape function[24] corrected for asymmetry[25] was used. A total of 775 reflections were used as input to create a Patterson map with the SHELXS86 program.[26] Only the position of the lead atom was derived. The inclusion of this atom, with the overall parameters obtained in the last cycle of the Le Bail refinement, reduced R_{wp} to 44.9% by refining only the scale factor. A difference-Fourier map revealed clearly the positions of the three phosphorus atoms, but no other atoms. Introducing P atoms and successive difference-Fourier maps revealed the positions of oxygens and carbons, reducing R_{wp} to 24.3%. At this stage, the positions of the located atoms were refined using soft constraints for the distances P–O [1.53(1) Å], P–C [1.80(1) Å], O···O [2.55(1) Å] and O···O [2.73(1) Å] to retain a reasonable geometry for the tetrahedral O_3PC groups. Initially, the weight factor for the soft constraints was high, -2000. Subsequently a new difference-Fourier map showed the position of the remaining atoms, except for the nitrogen atom, which was determined geometrically from the position of three carbon atoms. It was also necessary to include soft constraints for the atomic distances: C–N [1.47(1) Å], C···C [2.46(1) Å] and P···N [2.77(1) Å] to retain a good geometry for the organic moiety. For the last cycles, the weight of the soft constraints was reduced to a final value of -10. Although, without disordering, the samples preferred orientation is along the [010] direction, the use of Cab–O–Sil allowed removal of the preferred orientation. This was confirmed through the refined coefficient (0.99) of the March–Dollase[27] correction. One isotropic thermal parameter was refined for the lead atom, another for the three phosphorus atoms and a third for the other atoms. The final refinement converged to $R_{wP}=9.28\%$, $R_P=7.20\%$ and $R_F=2.67\%$; R factors are as defined by Rietveld[28] and Larson and Von Dreele.[22]

Final positional and thermal parameters are presented in Table 1 and bond lengths and angles are given in Table 2. The final observed, calculated and difference profiles are shown in

Table 1 Structural parameters for $Pb[(H_2O_3PCH_2)N(CH_2PO_3H)_2]$[a]

Atom	x	y	z	U_{iso}/Å^2
Pb1	0.13430(22)	0.37719(15)	0.24760(30)	0.0118(7)
N1	0.6747(12)	0.1677(7)	0.6879(22)	0.010(2)
P1	0.2781(10)	0.0535(6)	0.1297(15)	0.011(2)
O1	0.1618(15)	0.1711(8)	0.1477(26)	0.010
O2	0.2841(16)	0.0083(12)	0.8736(19)	0.010
O3	0.4560(11)	0.0678(12)	0.2662(26)	0.010
C1	0.7926(14)	0.0618(8)	0.7499(28)	0.010
P2	−0.0907(8)	0.2977(6)	−0.3837(14)	0.011
O4	0.9240(17)	0.3724(11)	0.8600(17)	0.010
O5	0.0454(13)	0.1864(9)	0.6293(27)	0.010
O6	0.9215(15)	0.3755(11)	0.4320(20)	0.010
C2	0.7130(11)	0.2399(11)	0.5291(20)	0.010
P3	0.4245(9)	0.3387(7)	0.8136(15)	0.011
O7	0.3762(16)	0.3950(13)	0.0410(22)	0.010
O8	0.2932(14)	0.2761(13)	0.6321(24)	0.010
O9	0.4576(18)	0.4443(11)	0.7024(26)	0.010
C3	0.6116(14)	0.2365(12)	0.8817(19)	0.010

[a]Space group, $a=8.5077(2)$, $b=11.2363(3)$, $c=5.9484(2)$ Å, $\alpha=98.802(2)$, $\beta=104.955(1)$, $\gamma=80.911(2)^\circ$, $V=538.71(3)$ Å^3, $Z=2$.

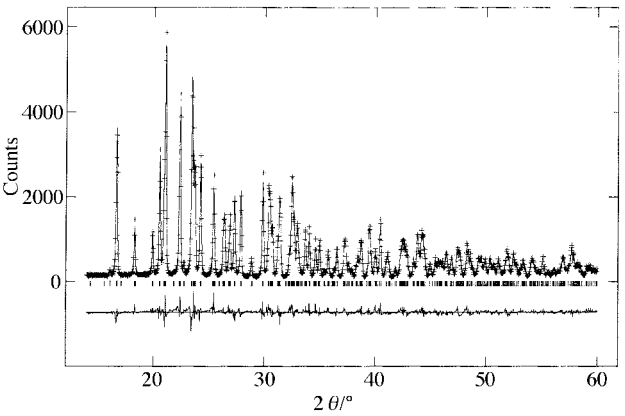

Fig. 4 Observed, calculated and difference X-ray powder diffraction profiles for $Pb[(H_2O_3PCH_2)N(CH_2PO_3H)_2]$. The tick marks are calculated 2θ angles for Bragg peaks.

Fig. 4. The coordination environments for TPA and the lead atom are shown in Fig. 5 where all atoms are labelled. The lead atom is surrounded by five oxygens, which define an irregular polyhedron with free space in which the lone pair of Pb^{2+} is located (Fig. 5 and 6). The Pb–O bond distances range between 2.29 and 2.70 Å, with a long interaction to a sixth oxygen at 2.92 Å. The molecular geometry of the nitrilotris(methylene)triphosphonic group is as expected with six tetrahedral groups: three phosphonates (CPO_3) and three methylenes, (PCH_2N), and a pyramidal NC_3 group. There are two crystallographically independent hydrogen phosphonate groups (P2 and P3) and a dihydrogen phosphonate group, P1.

This compound is layered and the packing of the layers along the *b*-axis is shown in Fig. 6. One layer (*ac* plane) is built up of TPA groups that link the lead atoms. The dihydrogen phosphonate group P1 is situated at the centre of a layer with the P1–O3H bond almost parallel to the *a*-axis direction and the P1–O2H bond almost parallel to the *c*-axis direction. P2–O5H hydrogen phosphonate groups point to small cavities inside the layer. The observed connectivity results in small cavities in which the hydrogen atoms of the $C1H_2$ methylene groups are situated. The hydrogens of the P3–O9H groups, the $C2H_2$ and $C3H_2$ groups point toward the interlayer space similarly to the lone pair of the Pb atoms.

The structure of this phosphonate is built with only weak electrostatic interactions between the layers, along the *b*-axis direction, *via* the lead atom of a given layer with the O4 atom of an adjacent layer (2.92 Å). The distance between two O9 atoms of the two layers is 3.16 Å, hence any hydrogen bond interaction, if present, is weak.

$Pb_2[(O_3PCH_2)N(CH_2PO_3H)_2]\cdot H_2O$. The X-ray powder diffraction pattern was auto-indexed by the TREOR90[19] program in a monoclinic unit cell with $a=7.359(1)$, $b=11.383(2)$, $c=7.254(1)$ Å, $\beta=100.36(2)^\circ$, $V=597.7$ Å^3, $Z=2$, V_{at} (non-H atoms)$=15.73$ Å^3 atom^{-1}, $M_{20}=36^{20}$ and $F_{20}=77$ (0.0091, 38).[21] The systematic absences were consistent with the centrosymmetric, space group $P2/n$. However, all attempts to solve the structure in $P2/n$ were unsuccessful. The model in this space group requires N to be placed in a special position with two hydrogen phosphonate groups being crystallographically equivalent. Then, we attempted to solve the structure in the non-centrosymmetric Pn space group. This choice was confirmed by the success in the structure solution process. The structure factor amplitudes were extracted from a limited region of the diffractogram ($13<2\theta<76.5^\circ$) using the Le Bail method implemented in the GSAS package. The pattern was fitted without any structural model by refining the overall parameters as described for **I**. A total number of 330 reflections (221 observed) were used as input in the SHELXS86 program[26] to create a Patterson map. Only the positions of the two crystallographically independent lead atoms, situated at (0, 0, 0) and (0.5, 0.21, 0.0), were derived. The inclusion of these two atoms, with the overall parameters obtained in the last cycle of the Le Bail refinement, reduced R_{wP} to 40.5% by refining only the scale factor. An initial difference Fourier map revealed the position of two P atoms reducing R_{wP} to 34.2%.

Table 2 Bond lengths (Å) and selected angles (°) for $Pb[(H_2O_3PCH_2)N(CH_2PO_3H)_2]$

Pb1–O1	2.291(10)	Pb1–O6	2.350(11)	Pb1–O8	2.658(14)
Pb1–O4	2.526(12)	Pb1–O7	2.701(13)	*Pb1–O4*	*2.919(14)*
N1–C1	1.458(6)	N1–C2	1.461(6)	N1–C3	1.460(7)
C1–N1–C2	115.7(5)	C1–N1–C3	114.8(7)	C2–N1–C3	115.7(6)
P1–O1	1.528(6)	O1–P1–O2	111.6(5)	O1–P1–C1	108.6(5)
P1–O2	1.542(6)	O1–P1–O3	112.7(6)	O2–P1–C1	109.1(5)
P1–O3	1.542(6)	O2–P1–O3	106.5(8)	O3–P1–C1	108.1(5)
P1–C1	1.818(6)				
P2–O4	1.545(6)	O4–P2–O5	110.2(5)	O4–P2–C2	108.5(5)
P2–O5	1.562(6)	O4–P2–O6	111.5(5)	O5–P2–C2	107.6(5)
P2–O6	1.535(6)	O5–P2–O6	109.8(5)	O6–P2–C2	109.2(5)
P2–C2	1.809(6)				
P3–O7	1.530(7)	O7–P3–O8	115.2(10)	O7–P3–C3	109.3(5)
P3–O8	1.517(7)	O7–P3–O9	106.2(1)	O8–P3–C3	110.7(5)
P3–O9	1.539(7)	O8–P3–O9	106.5(10)	O9–P3–C3	108.6(5)
P3–C3	1.802(7)				
N–C1–P1	116.6(5)	N–C2–P2	117.5(6)	N–C3–P3	118.3(6)

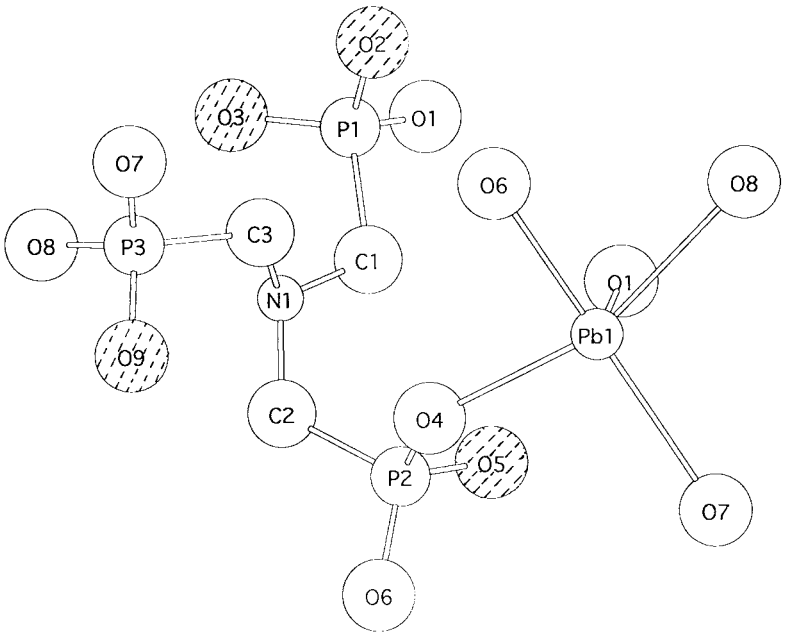

Fig. 5 Coordination geometry in $Pb[(H_2O_3PCH_2)N(CH_2PO_3H)_2]$ with atoms labelled. The oxygens of the hydrogen phosphonate groups are shaded.

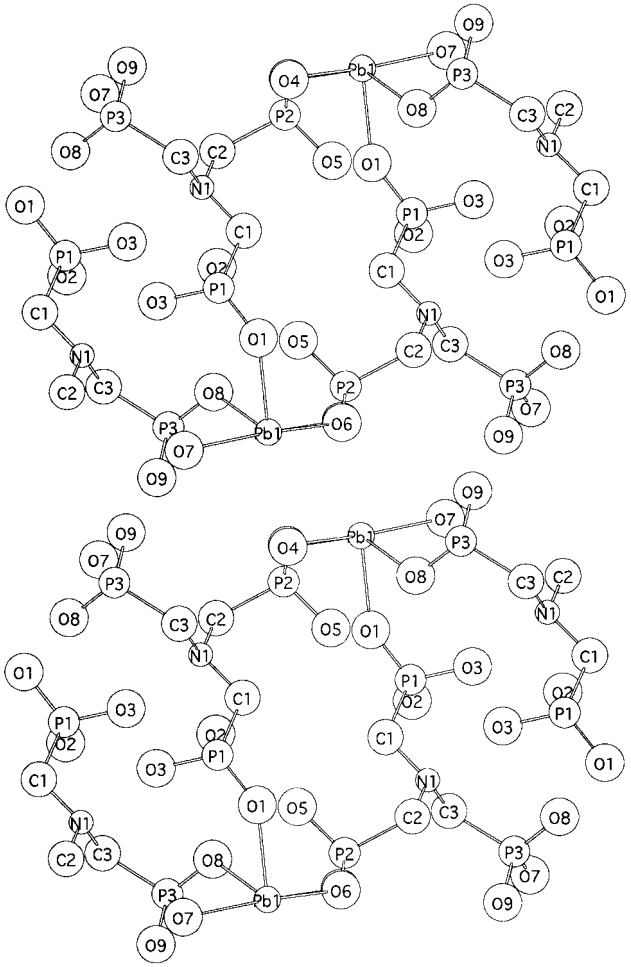

Fig. 6 [001] View of the crystal structure of $Pb[(H_2O_3PCH_2)N(CH_2PO_3H)_2]$ with atoms labelled (*b*-axis vertical).

A new difference Fourier map gave the position for the third P atom as well as several oxygen atoms. At this point, only the phosphonate P3 group was complete; therefore a following step was to refine the position of the two lead atoms together with this phosphonate group by using soft constraints for the

Table 3 Structural parameters for $Pb_2[(H_2O_3PCH_2)N(CH_2PO_3)_2]\cdot H_2O$[a]

Atom	*x*	*y*	*z*	U_{iso}/Å^2
Pb1	0.0372(11)	−0.00897(26)	−0.0617(12)	0.0091(1)
Pb2	0.5875(11)	0.19346(19)	−0.0303(12)	0.011(1)
N1	0.1344(15)	0.2977(12)	0.3374(14)	0.024(4)
P1	0.9645(15)	0.0899(10)	0.4196(22)	0.034(4)
O1	0.6146(28)	−0.0218(18)	0.840(4)	0.024
O2	0.926(4)	0.0301(17)	0.5998(29)	0.024
O3	0.7850(25)	0.0997(21)	0.2735(32)	0.024
C1	1.0504(34)	0.2367(13)	0.4796(24)	0.024
P2	0.1044(18)	0.2600(11)	−0.0448(13)	0.034
O4	0.2261(35)	0.1964(22)	0.8330(20)	0.024
O5	1.113(4)	0.3933(12)	0.9344(26)	0.024
O6	0.9022(22)	0.2147(24)	−0.0944(34)	0.024
C2	0.1906(24)	0.2196(15)	0.1972(14)	0.024
P3	0.5088(14)	0.3038(12)	0.4761(19)	0.034
O7	0.5214(32)	0.2187(23)	0.3120(33)	0.024
O8	0.6641(16)	0.3958(17)	0.497(4)	0.024
O9	0.5338(33)	0.2346(23)	0.6599(29)	0.024
C3	0.2871(14)	0.3781(11)	0.4211(32)	0.024
O10	0.559(5)	0.4828(26)	0.869(5)	0.024

[a]Space group, *Pn*, $a=7.3614(2)$, $b=11.3889(2)$, $c=7.2541(2)$ Å, $\beta=100.389(2)^\circ$, $V=598.20(2)$ Å^3, $Z=2$.

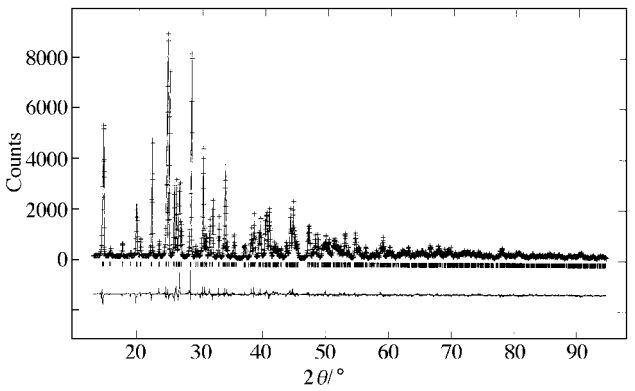

Fig. 7 Observed, calculated and difference X-ray powder diffraction profiles for $Pb_2[(O_3PCH_2)N(CH_2PO_3H)_2]\cdot H_2O$. The tick marks are calculated 2θ angles for Bragg peaks.

Table 4 Bond lengths (Å) and selected angles (°) for $Pb_2[(H_2O_3PCH_2)N(CH_2PO_3)_2]\cdot H_2O$

Pb1–O2	2.485(22)	*Pb1–O1*	*2.885(28)*	*Pb1–O7*	*2.973(27)*
Pb1–O3	2.571(25)	*Pb1–O4*	*2.893(29)*	*Pb1–O9*	*3.052(31)*
Pb1–O6	2.730(29)	*Pb1–O2*	*2.901(27)*	*Pb1–O1*	*3.067(22)*
Pb1–O7	2.554(31)				
Pb2–O1	2.648(27)	Pb2–O6	2.455(22)	*Pb2–O2*	*3.031(25)*
Pb2–O3	2.637(21)	Pb2–O7	2.631(23)	*Pb2–O10*	*3.374(31)*
Pb2–O4	2.667(27)	Pb2–O9	2.264(19)		
N1–C1	1.470(6)	N1–C2	1.466(6)	N1–C3	1.491(6)
C1–N1–C2	114.0(6)	C1–N1–C3	112.7(6)	C2–N1–C3	111.7(6)
P1–O1	1.546(5)	O1–P1–O2	110.4(5)	O1–P1–C1	108.1(4)
P1–O2	1.545(5)	O1–P1–O3	111.1(5)	O2–P1–C1	108.2(4)
P1–O3	1.542(5)	O2–P1–O3	110.4(5)	O3–P1–C1	108.5(4)
P1–C1	1.812(5)				
P2–O4	1.549(5)	O4–P2–O5	111.7(5)	O4–P2–C2	107.3(4)
P2–O5	1.528(5)	O4–P2–O6	109.9(5)	O5–P2–C2	109.5(4)
P2–O6	1.555(5)	O5–P2–O6	111.1(5)	O6–P2–C2	107.0(4)
P2–C2	1.815(5)				
P3–O7	1.550(5)	O7–P3–O8	110.7(5)	O7–P3–C3	107.3(4)
P3–O8	1.538(5)	O7–P3–O9	110.4(5)	O8–P3–C3	109.0(4)
P3–O9	1.543(5)	O8–P3–O9	111.1(5)	O9–P3–C3	109.9(4)
P3–C3	1.815(5)				
N–C1–P1	116.1(5)	N–C2–P2	115.1(6)	N–C3–P3	112.6(5)

tetrahedral distances of the O_3PC group (as for **I**). The initial weight for the soft constraints was −2000. This procedure reduced R_{wP} to 20.2%. Successive difference Fourier maps and soft constrained refinements revealed the atomic positions of the full structure. It was also necessary to use soft constraints in the C–N, C···C and P···N distances as for **I**. Subsequent refinements of overall parameters, atomic positions and reducing the soft constraints weight gradually to −50, gave the final factors: $R_{wP}=12.51\%$, $R_P=9.38\%$ and $R_F=4.45\%$. The refined coefficient of the March–Dollase[27] correction for the preferred orientation was 0.919(2), along the [010] direction. An isotropic thermal parameter was refined for each Pb atoms, another for P atoms and a third for the remaining atoms.

The final observed, calculated and difference profiles are given in Fig. 7. Positional parameters are given in Table 3 and bond lengths and selected angles in Table 4. The structure is formed by 19 non-hydrogen atoms all in general positions. The coordination environments for TPA and the lead atoms are given in Fig. 8 in which atoms are labelled. The crystal structure contains two crystallographically independent Pb atoms. Their environments consist of six oxygen atoms for Pb2 and four atoms for Pb1 and both define two irregular polyhedra due to the lone pair of Pb^{2+} (Fig. 8). The Pb2–O bond distances range between 2.26 and 2.67 Å, with two interactions to O2 and O10 at 3.03 and 3.37 Å, respectively (Table 4). The environment for Pb1 is even more distorted with four short distances ranging between 2.49 and 2.73 Å and the other six interactions to oxygens ranging between 2.89 and 3.05 Å (Table 4). These distances are too large to be considered as bond distances but they are not negligible interactions. The molecular geometry of TPA groups is as expected and quite similar to that found in **I**. However there are two hydrogen phosphonate groups, P2–O5 and P3–O8. These oxygens are not bonded to the lead atoms.

This compound is also layered and the packing of the layers down the *c*-axis is shown in Fig. 9. One layer (*ac* plane) is built up of TPA units that bond the lead atoms. Conversely to **I**, inside the layers of **II**, $CP1O_3$ groups are deprotonated and there are no intralayer cavities in this structure. There is only some space for the lone pairs of Pb1 and Pb2. Both hydrogen phosphonate groups, P2–O5H and P3–O8H, point to the interlamellar space. The hydrogens of the methylene

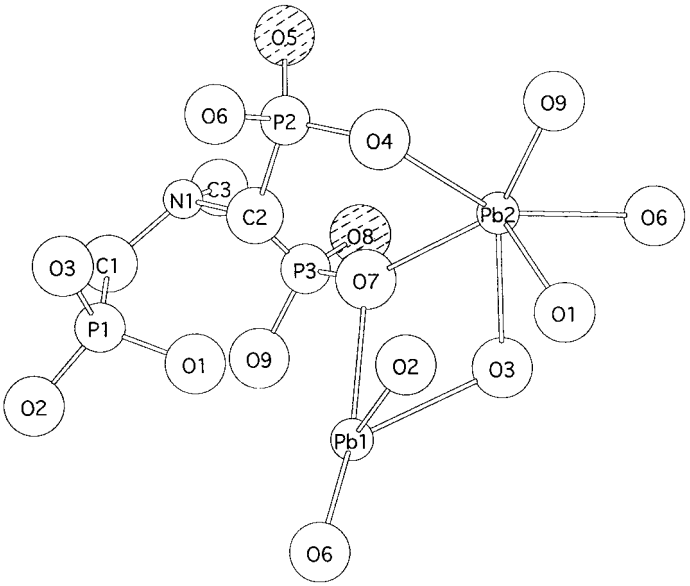

Fig. 8 Coordination geometry in $Pb_2[(O_3PCH_2)N(CH_2PO_3H)_2]\cdot H_2O$ with atoms labelled.

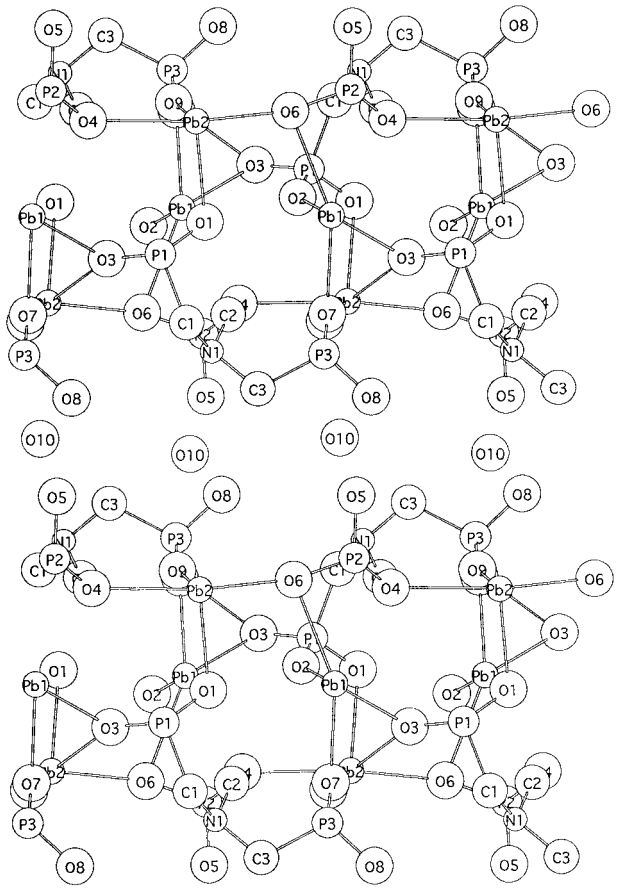

Fig. 9 [001] View of the crystal structure of $Pb_2[(O_3PCH_2)N(CH_2PO_3H)_2]\cdot H_2O$ with atoms labelled (*b*-axis vertical).

groups $C2H_2$ and $C3H_2$ are also projected to the interlamellar space. The layers of **II** are held together by hydrogen-bonding along the *b*-axis. The water molecule is located in the interlayer space and interacts through H-bonding with O8 of an adjacent layer at 3.10 Å and the nitrogen of a second layer at 2.58 Å. The hydrogen phosphonate group P2–O5H interacts very weakly by H-bonding, with an O5···O10 distance of 3.54 Å.

When **II** is heated above 160 °C the water molecule is lost, resulting in $Pb_2[(O_3PCH_2)N(CH_2PO_3H)_2]$ **III** which crystallises in an orthorhombic unit cell with $a=10.873(4)$, $b=11.740(4)$, $c=9.328(4)$ Å, $V=1190.8$ Å^3, $M_{20}=14^{20}$ and $F_{20}=23$ (0.016, 55).[21] The similar lattice cell parameters, compared with **II**, suggest a strongly related layered structure. In fact, the thermodiffractometric study indicates that the water loss does not strongly affect the parameters, as the powder patterns of **II** and **III** are very similar.

Conclusions

In this paper we have studied two new triphosphonates: $Pb[(H_2O_3PCH_2)N(CH_2PO_3H)_2]$ **I** and $Pb_2[(O_3PCH_2)N(CH_2PO_3H)_2]\cdot H_2O$ **II**. Although, both compounds are layered, **I** shows small cavities in the inorganic layer, where the hydroxy groups of two hydrogen phosphonate groups are located. **II** also shows a layered structure with the water molecule between layers and the hydrogen phosphonate groups pointing to the interlamellar space. We have also studied the possibility of exchanging the protons of the different hydrogen phosphonate groups in **I** and **II**. Ion exchange does not take place for either **I** or **II**, although a transformation of **I**→**II** was observed at sufficiently high pH in water. **II** dehydrates topotactically above 160 °C to give **III**.

Acknowledgements

This work was supported by the research grants FQM-113 of Junta de Andalucía (Spain).

References

1 A. Clearfield, *Prog. Inorg. Chem.*, 1998, **47**, 371; S. Drumel, V. Penicaud, D. Deniaud and B. Bujoli, *Trends Inorg. Chem.,* 1996, **4**, 13.
2 G. Alberti, U. Costantino, S. Allulli and N. Tomasini, *J. Inorg. Nucl. Chem.*, 1978, **40**, 1113; M. B. Dines and P. DiGiacomo, *Inorg. Chem.*, 1981, **20**, 92.
3 G. Alberti, M. Casciola, U. Costantino and R. Vivani, *Adv. Mater.*, 1996, **8**, 291.
4 D. Cunningham, P. J. Hennelly and T. Deeny, *Inorg. Chim. Acta*, 1979, **37**, 95; G. Cao, H. Lee, V. M. Lynch and T. E. Mallouk, *Inorg. Chem.*, 1988, **27**, 2781.
5 K. J. Martin, P. J. Squattrito and A. Clearfield, *Inorg. Chim. Acta*, 1988, **155**, 7; G. Cao, H. Lee, V. M. Lynch and T. E. Mallouk, *Solid State Ionics*, 1988, **26**, 63; G. Cao, H. Lee, V. M. Lynch, J. S. Swinnea and T. E. Mallouk, *Inorg. Chem.,* 1990, **29**, 2112.
6 Y. Zhang and A. Clearfield, *Inorg. Chem.*, 1992, **31**, 2821; C. Bhardwaj, H.-L. Hu and A. Clearfield, *Inorg. Chem.*, 1993, **32**, 4294; A. Cabeza, M. A. G. Aranda, M. Martinez-Lara, S. Bruque and J. Sanz, *Acta Crystallogr.*, *Sect. B*, 1996, **52**, 982.
7 B. Bujoli, P. Palvadeau and J. Rouxel, *Chem. Mater.*, 1990, **2**, 582.
8 R. Wang, Y. Zhang, H. Hu, R. R. Frausto and A. Clearfield, *Chem. Mater.*, 1992, **4**, 864.
9 A. Cabeza, M. A. G. Aranda, S. Bruque, M. D. Poojary, A. Clearfield and J. Sanz, *Inorg. Chem.*, 1998, 37, 4168.
10 B. Bujoli, P. Palvadeau and J. Rouxel, *Chem. Mater.*, 1990, **2**, 582; D. M. Poojary, Y. P. Zhang, B. Zhang and A. Clearfield, *Chem. Mater*., 1995, **7**, 822; D. Grohol, M. A. Subramanian, M. D. Poojary and A. Clearfield, *Inorg. Chem.*, 1996, **35**, 5264; D. Grohol and A. Clearfield, *J. Am. Chem. Soc.*, 1997, **119**, 4662.
11 J. Le Bideau, C. Payen, P. Palvadeau and B. Bujoli, *Inorg. Chem.*, 1994, **33**, 4885; S. Drumel, P. Janvier, D. Deniaud and B. Bujoli, *J. Chem. Soc.*, *Chem. Commun.*, 1995, 1051;. K. Maeda, J. Akimoto, Y. Kiyozumi and F. Mizukami, *Angew. Chem.*, *Int. Ed. Engl.*, 1995, **34**, 1199; K. Maeda, J. Akimoto, Y. Kiyozumi and F. Mizukami, *J. Chem. Soc.*, *Chem. Commun.*, 1995, 1033; M. D. Poojary, A. Cabeza, M. A. G. Aranda, S. Bruque and A. Clearfield, *Inorg. Chem*., 1996, **35**, 1468; M. D. Poojary, D. Grohol and A. Clearfield, *Angew. Chem.*, *Int. Ed. Engl.*, 1995, **34**, 1508.
12 F. Fredoueil, V. Penicaud, M. Bujoli-Doeuff and B. Bujoli, *Inorg. Chem.*, 1997, **36**, 4702.
13 M. B. Dines, R. E. Cooksey, P. C. Griffith and R. H. Lane, *Inorg. Chem.*, 1983, **22**, 1003; G. Alberti, R. Costantino, F. Marmottini and Z. P. Vivaniv, *Angew. Chem.*, *Int. Ed. Engl*., 1993, **32**, 1357; G. Alberti, F. Marmottini, S. Murcia-Mascaros and R. Vivani, *Angew. Chem.*, *Int. Ed. Engl*., 1994, **33**, 1594; M. E. Thompson, *Chem. Mater.*, 1994, **6**, 1168; D. M. Poojary, B. Zhang, P. Bellinghausen and A. Clearfield, *Inorg. Chem.*, 1996, **35**, 5254; D. M. Poojary, B. Zhang, P. Bellinghausen and A. Clearfield, *Inorg. Chem.*, 1996, **35**, 4942.
14 B. Bujoli, A. Courilleau, P. Palvadeau and J. Rouxel, *Eur. J. Solid State Inorg. Chem.*, 1992, **92**, 171; S. Drumel, M. Bujoli-Doueff, P. Janvier and B. Bujoli, *New J. Chem.*, 1995, **19**, 239; S. Drumel, P. Janvier, P. Barboux, M. Bujoli-Doeuff and B. Bujoli, *Inorg. Chem.*, 1995, **34**, 148; P. Janvier, S. Drumel, P. Piffard, and B. Bujoli, *C. R. Acad. Sci. Paris*, *Ser. II*, 1995, **320**, 29.
15 R. LaDuca, D. Rose, J. R. D. DeBord, R. C. Haushalter, C. J. O'Connor and J. Zubieta, *J. Solid State Chem.,* 1996, **123**, 408 and references therein.
16 A. Cabeza, M. A. G. Aranda, M. Martínez-Lara and S. Bruque, *Mater. Sci. Forum*, 1996, **228**, 165.
17 A. Cabeza, E. R. Losilla, H.S. Martinez-Tapia, S. Bruque and M. A. G. Aranda, *Adv. X-ray Anal.*, 1998, submitted.
18 Y. Zhang, K. J. Scott and A. Clearfield, *Chem. Mater*., 1993, **5**, 495.
19 P. E. Werner, L. Eriksson and M. Westdahl, *J. Appl. Crystallogr.*, 1985, **18**, 367.
20 P. M. Wolff, *J. Appl. Crystallogr.*, 1968, **1**, 108.
21 G. S. Smith and R. L. Snyder, *J. Appl. Crystallogr.*, 1979, **12**, 60.
22 A. C. Larson and R. B. von Dreele, (Program version: PC). Los Alamos National Lab. Rep. No. LA-UR-86–748, 1994.

23 A. Le Bail, H. Duroy and J. L. Fourquet, *Mater. Res. Bull.*, 1988, **23**, 447.
24 P. Thompson, D. E. Cox and J. B. Hasting, *J. Appl. Crystallogr.*, 1987, **20**, 79.
25 L. W. Finger, D. E. Cox and A. P. Jephcoat, *J. Appl. Crystallogr.*, 1994, **27**, 892.
26 G. M. Sheldrick, SHELXS86. Program for the Solution of Crystal Structures, University of Göttingen, Germany, 1985.
27 W. A. Dollase, *J. Appl. Crystallogr.*, 1986, **19**, 267.
28 H. M. Rietveld, *J. Appl. Crystallogr.*, 1969, **2**, 65.

Paper 8/05609I